Short Article

Cell Metabolism

mTORC1 Regulates Mitochondrial Integrated Stress Response and Mitochondrial Myopathy Progression

Graphical Abstract

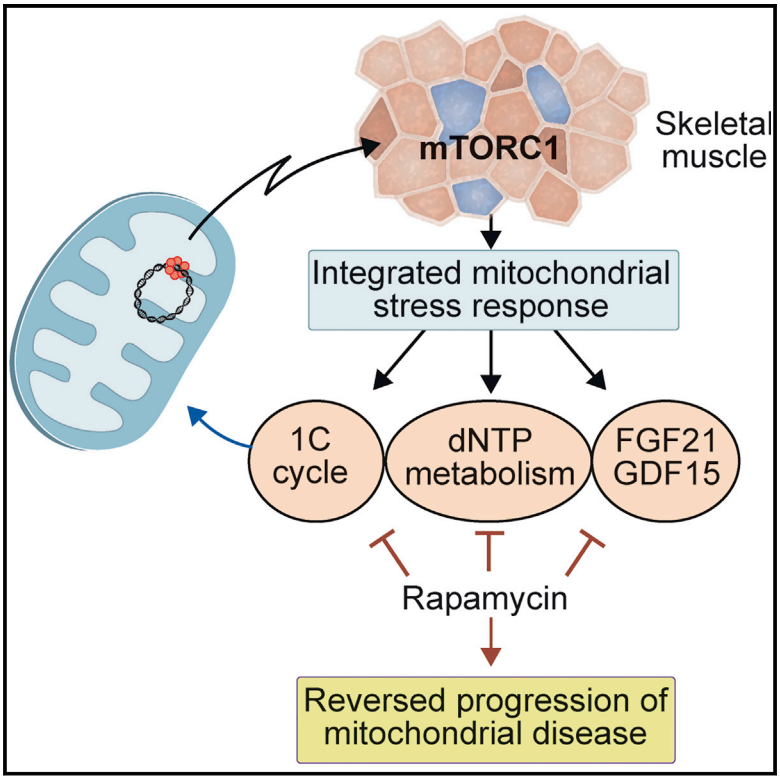

Highlights

- mtDNA replication defect activates mTORC1 and integrated mitochondrial stress response
- mTORC1 upregulates mitochondrial 1C-cycle, FGF21, and UPRmt in mitochondrial disease
- mTORC1 contributes to ragged-red fiber formation in mitochondrial myopathy
- Rapamycin reverts progression of mitochondrial myopathy in mice

Authors

Nahid A. Khan, Joni Nikkanen, Shuichi Yatsuga, ..., Alberto Pessia, Vidya Velagapudi, Anu Suomalainen

Correspondence

anu.wartiovaara@helsinki.fi

In Brief

Khan et al. report that mtDNA replication defect activates mTORC1, which drives an integrated mitochondrial stress response through ATF4 activation, inducing de novo nucleotide and serine synthesis, 1C-cycle, and FGF21 and GDF15 production. Downregulation of this response by rapamycin cured hallmarks of mitochondrial myopathy in mice.

Khan et al., 2017, Cell Metabolism *26*, 419–428
August 1, 2017 © 2017 Elsevier Inc.
http://dx.doi.org/10.1016/j.cmet.2017.07.007

CellPress

Cell Metabolism
Short Article

mTORC1 Regulates Mitochondrial Integrated Stress Response and Mitochondrial Myopathy Progression

Nahid A. Khan,[1] Joni Nikkanen,[1] Shuichi Yatsuga,[1,2] Christopher Jackson,[1] Liya Wang,[3] Swagat Pradhan,[1] Riikka Kivelä,[4] Alberto Pessia,[5] Vidya Velagapudi,[5] and Anu Suomalainen[1,6,7,8,*]
[1]Research Programs Unit, Molecular Neurology, University of Helsinki, 00290 Helsinki, Finland
[2]Department of Pediatrics and Child Health, Kurume University School of Medicine, Fukuoka, Japan
[3]Department of Anatomy, Physiology, and Biochemistry, Swedish University of Agricultural Sciences, 75007 Uppsala, Sweden
[4]Research Programs Unit, Translational Cancer Biology, University of Helsinki, 00290 Helsinki, Finland
[5]Metabolomics Unit, Institute for Molecular Medicine Finland, University of Helsinki, 00290 Helsinki, Finland
[6]Department of Neurology, Helsinki University Hospital, 00290 Helsinki, Finland
[7]Neuroscience Center, University of Helsinki, 00790 Helsinki, Finland
[8]Lead Contact
*Correspondence: anu.wartiovaara@helsinki.fi
http://dx.doi.org/10.1016/j.cmet.2017.07.007

SUMMARY

Mitochondrial dysfunction elicits various stress responses in different model systems, but how these responses relate to each other and contribute to mitochondrial disease has remained unclear. Mitochondrial myopathy (MM) is the most common manifestation of adult-onset mitochondrial disease and shows a multifaceted tissue-specific stress response: (1) transcriptional response, including metabolic cytokines FGF21 and GDF15; (2) remodeling of one-carbon metabolism; and (3) mitochondrial unfolded protein response. We show that these processes are part of one integrated mitochondrial stress response (ISRmt), which is controlled by mTORC1 in muscle. mTORC1 inhibition by rapamycin downregulated all components of ISRmt, improved all MM hallmarks, and reversed the progression of even late-stage MM, without inducing mitochondrial biogenesis. Our evidence suggests that (1) chronic upregulation of anabolic pathways contributes to MM progression, (2) long-term induction of ISRmt is not protective for muscle, and (3) rapamycin treatment trials should be considered for adult-type MM with raised FGF21.

INTRODUCTION

Mitochondrial disorders are the most common inherited metabolic disorders, caused by defects in genes encoded by either mitochondrial DNA (mtDNA) or nuclear DNA (Chinnery, 2015; Koopman et al., 2016; Young and Copeland, 2016). They present with an exceptional clinical and genetic variability, the molecular basis of which is still unknown. We have previously generated a mouse model (Deletor mouse) for mitochondrial myopathy (MM) carrying a dominant patient mutation in the mitochondrial replicative helicase Twinkle (Tyynismaa et al., 2005). These mice live a normal lifespan, but accumulate multiple mtDNA deletions in their postmitotic tissues and develop slowly progressive respiratory chain (RC) deficiency in their skeletal muscle, heart, and brain at 1 year of age, replicating the typical molecular findings in adult patients with Twinkle mutations (Spelbrink et al., 2001; Suomalainen et al., 1992). The morphological hallmarks of MM in Deletor mice and in patients are RC-deficient muscle fibers, including cytochrome *c* oxidase (COX)-negative, succinate dehydrogenase (SDH)-positive fibers with subsarcolemmal mitochondrial accumulations, so-called ragged-red fibers (RRFs). These fibers show enlarged mitochondria with aberrant cristae and inclusions and prevalent mitophagosomes (Olson et al., 1972; Suomalainen et al., 1992; Tyynismaa et al., 2005).

Despite the slow progression of MM in mice and patients, the disease induces a robust transcriptional and metabolic stress response in the affected tissues, notably in the skeletal muscle, involving components of amino acid starvation response, mitochondrial unfolded protein response (UPRmt), and remodeled folate-driven one-carbon (1C) metabolism (Khan et al., 2014; Nikkanen et al., 2016; Tyynismaa et al., 2010). The majority of the upregulated genes in Deletor muscle harbor an amino acid starvation response element (AARE) in their upstream regulatory regions. This element is a binding site for ATF transcription factors (Nargund et al., 2012; Taylor et al., 2014; Tyynismaa et al., 2010). One of the genes regulated by the "AARE response" encodes for fibroblast growth factor 21 (FGF21), which is a metabolic cytokine secreted to blood in fasting, but also from affected muscle fibers of MM patients and mice (Suomalainen et al., 2011; Tyynismaa et al., 2010). Indeed, FGF21 is a clinical serum biomarker for MM (Suomalainen et al., 2011), especially for diseases caused by defects in mitochondrial translation (mtDNA deletions and translation machinery defects) (Lehtonen et al., 2016).

The AARE response also induces the expression of methylene tetrahydrofolate dehydrogenase 2 (MTHFD2), which is the rate-limiting enzyme of mitochondrial folate cycle and is highly expressed in MM (Christensen and MacKenzie, 2006; Jain et al., 2012; Nilsson et al., 2014; Tyynismaa et al., 2010). MTHFD2 induction in Deletor mice is associated with imbalance in folate-driven 1C metabolism, aberrant nucleotide synthesis,

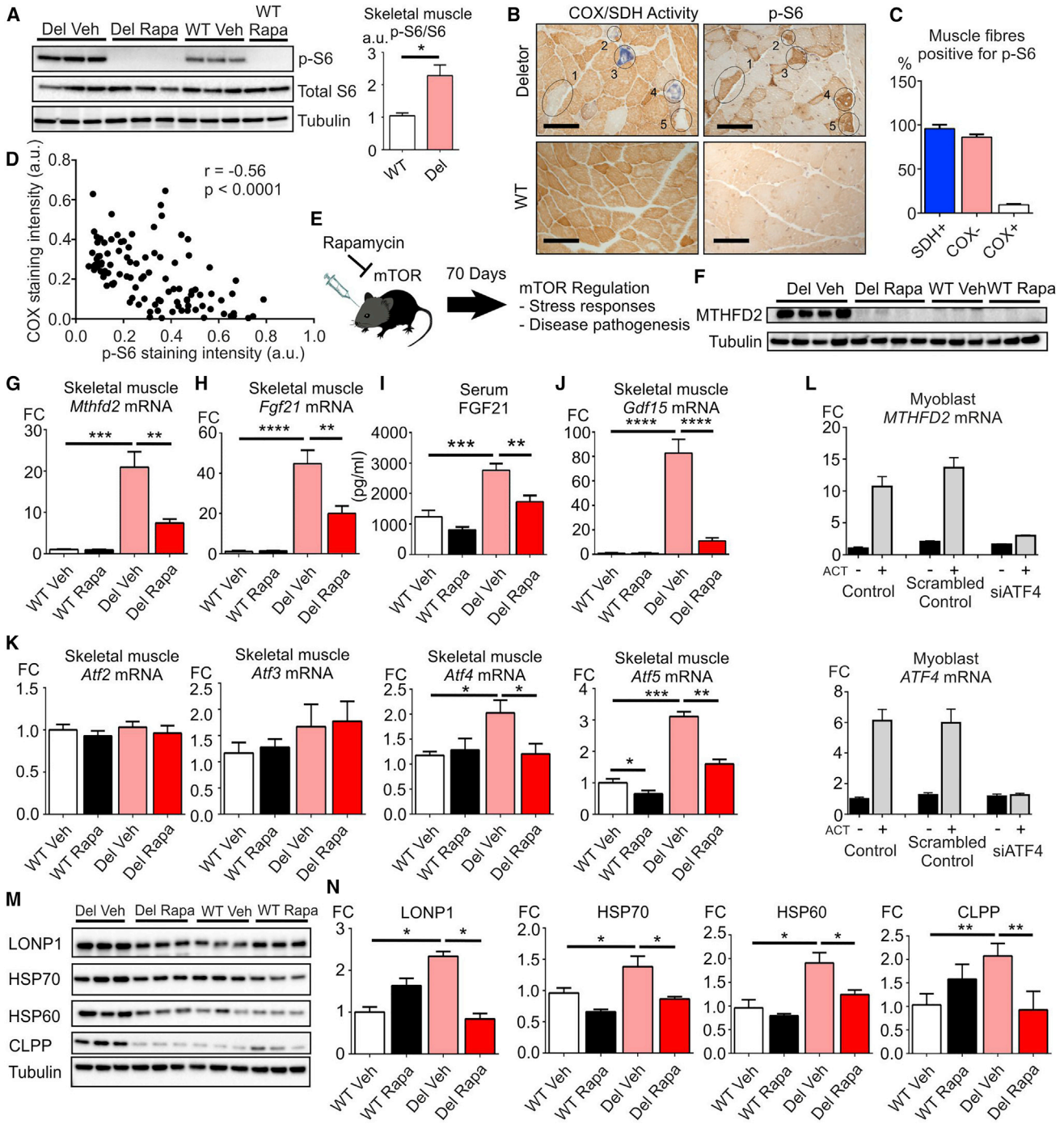

Figure 1. mTORC1 Is Activated in Affected Muscle Fibers in MM

(A) Total S6 and phosphorylated S6 (p-S6) protein amounts in skeletal muscle. Western blot analysis. Right: blot quantification.

(B) RC activity and S6-phosphorylation in skeletal muscle. Histochemical activity analysis of cytochrome *c* oxidase (COX; brown) and succinate dehydrogenase (SDH; blue) and p-S6 immunostaining in consecutive sections. Numbers identify the same fibers, in consecutive sections. Scale bars, 100 μm.

(C) Amount of p-S6-positive muscle fibers (500 fibers counted per mouse; n = 6).

(D) COX and p-S6 staining intensities in 100 fibers, consecutive sections.

(E) Study design of Deletor and WT mice.

(F) MTHFD2 protein amount in skeletal muscle, compared to tubulin as a loading control.

(G) *Mthfd2* mRNA expression in skeletal muscle.

(H) *Fgf21* mRNA expression in skeletal muscle.

(I) Serum FGF21 protein; ELISA quantification.

(legend continued on next page)

imbalanced dNTP pools, and induction of de novo serine and glutathione synthesis (Nikkanen et al., 2016). These observations show that a primary mtDNA replication defect induces major transcriptional and metabolic changes in the affected tissues. Whether these responses are consequences of conflicting signaling induced by the disease, or part of a coordinated response to protect the affected cells, is unknown.

Mechanistic (mammalian) target of rapamycin (mTOR) complex I (mTORC1) is a major regulator of metabolic signaling, integrating environmental cues and signals to organismal growth and homeostasis by transitioning between anabolic and catabolic states (Saxton and Sabatini, 2017). mTORC1 stimulates de novo synthesis of proteins, nucleotides, and lipids, and inhibits autophagy (Shimobayashi and Hall, 2014), overlapping with pathways induced in MM (Nikkanen et al., 2016). Furthermore, mTORC1 inhibition has been proposed to delay progression of brain pathology of mice with RC complex I NDUFS4-subunit knockout, and mTORC1 activation has also been linked to RC dysfunction in an induced pluripotent cell model (Johnson et al., 2013; Zheng et al., 2016). However, the roles of mTORC1 in mitochondrial disease in general are still poorly understood in vivo. We asked whether mTORC1 has a role in the induction of the various responses and progression of MM, the most common form of adult-onset mitochondrial disease. We report here that mTORC1 is a key upstream regulator of all the transcriptional and metabolic stress responses identified in muscle-manifesting mitochondrial disease. Furthermore, rapamycin, a drug inhibiting the kinase function of mTORC1 (Chen et al., 1995; Sabatini et al., 1994), remarkably reversed MM progression.

RESULTS AND DISCUSSION

RC Deficiency Induces mTORC1 in MM

We studied 22-month-old Deletor male mice (ubiquitously expressing dominant duplication of 13 aa in Twinkle helicase), which manifest with a robust MM with all its histological and molecular hallmarks (Tyynismaa et al., 2005, 2010). We found these mice to have increased phosphorylation of S6 ribosomal protein (p-S6) and S6 kinase (p-S6K), downstream targets of mTORC1 kinase (Ma and Blenis, 2009; Saxton and Sabatini, 2017), in their quadriceps femoris muscle, with unchanged total S6 and S6K amounts (Figures 1A and S1A). Muscle histology showed that induction of p-S6 was robust, but mosaic, significantly correlating with severity of RC deficiency ($p < 0.0001$) and especially prominent in fibers with the most severe RC deficiency: 95% of COX-negative and SDH-positive fibers with mitochondrial proliferation (typical for advanced RC deficiency), 86% of COX negative, and 10% of those with normal RC activities were positive for p-S6 (Figures 1B–1D). As RC deficiency may be regional, the p-S6-positive fibers with normal COX activity may be COX deficient in parts of the fibers that are outside the muscle cross-section. The data demonstrate that a primary mtDNA replication insult activates mTORC1 in skeletal muscle, and the induction correlates with the severity of the defect.

Rapamycin Treatment Silences Mitochondrial Folate Cycle, AARE, and UPRmt Stress Responses in Mitochondrial Disease

To evaluate the relationship between mTORC1 activation and disease responses, we treated 22-month-old Deletors with an mTORC1 inhibitor, rapamycin (rapa), intraperitoneally 8 mg/kg/day for 70 days (Figure 1E). This dosage provides a steady-state blood concentration of 45 ng/mL in mice (Johnson et al., 2013), similar to recommended maintenance concentrations in human patients (3–30 ng/mL). The inactivation of mTORC1 was efficient: p-S6 decreased in Deletor and wild-type (WT) muscles (Figures 1A and S1B). The treatment did not affect mTORC2 in muscle, judged by unchanged phosphorylation status of AKT1 (aa 308, 473, and 450; Figure S1C).

The induction of AARE-regulated *Mthfd2* and *Fgf21* is a major sign of MM, and their expression levels correlate with disease progression (Figures 1F–1H) (Tyynismaa et al., 2010). Rapa intervention reduced both transcript levels in the muscle, and MTHFD2 protein expression was decreased to WT level (Figures 1F–1H). Serum FGF21 level was also significantly decreased (Figure 1I), as was the expression of growth differentiation factor 15 (*Gdf15*), a cytokine induced in mtDNA expression diseases (Lehtonen et al., 2016; Yatsuga et al., 2015) (Figure 1J). The data indicate that inhibition of mTORC1 normalizes molecular markers of MM: metabolic cytokines and folate cycle.

The ATF family members that mediate mitochondrial disease-related AARE response are unknown. *Atf4* and *Atf5* were significantly induced in Deletor muscle, and rapa decreased their expression (Figure 1K), whereas *Atf2* and *Atf3* were not significantly changed and were not affected by rapa (Figure 1K). To study the induction in a myoblast culture system, we used actinonin, a mitochondrial translation inhibitor (Richter et al., 2015). We found actinonin to induce the expression of *MTHFD2* and *ATF4* in human myoblasts, and this response was abolished with downregulation of ATF4 by small interfering RNA (siRNA) (Figure 1L), strongly pointing to ATF4 being an upstream inducer of the AARE response.

ATFs have been previously linked to UPRmt and the components have been characterized in detail in the worm *C. elegans* (Haynes et al., 2007). The mammalian homologs of the worm UPRmt—HSP60, HSP70, LONP1, and CLPP —showed 1.5- to 2-fold induction in Deletor muscle. All these proteins were suppressed after rapa treatment in the Deletor mice (Figures 1M and 1N).

(J) *Gdf15* mRNA expression in skeletal muscle.
(K) *Atf2*, *Atf3*, *Atf4*, and *Atf5* mRNA expressions in skeletal muscle.
(L) *MTHFD2* and *ATF4* mRNA expression in human cultured myoblasts after 16 hr of actinonin treatment.
(M) LONP1, HSP60, HSP70, and CLPP protein amounts in skeletal muscle.
(N) Quantification of signals in (M).
In (G)–(K), WT vehicle, n = 7; WT rapa, n = 7; Deletor vehicle, n = 9; Deletor rapa, n = 9. All data are shown as mean with SEM. Statistical testing was done by using Student's t test; *$p \leq 0.05$, **$p \leq 0.01$, ***$p \leq 0.001$, ****$p \leq 0.0001$.
FC, fold change; Rapa, rapamycin; Del, Deletor; WT, wild-type mice; Veh, vehicle; a.u., arbitrary units; ACT, Actinonin; mTOR, mammalian target of rapa.

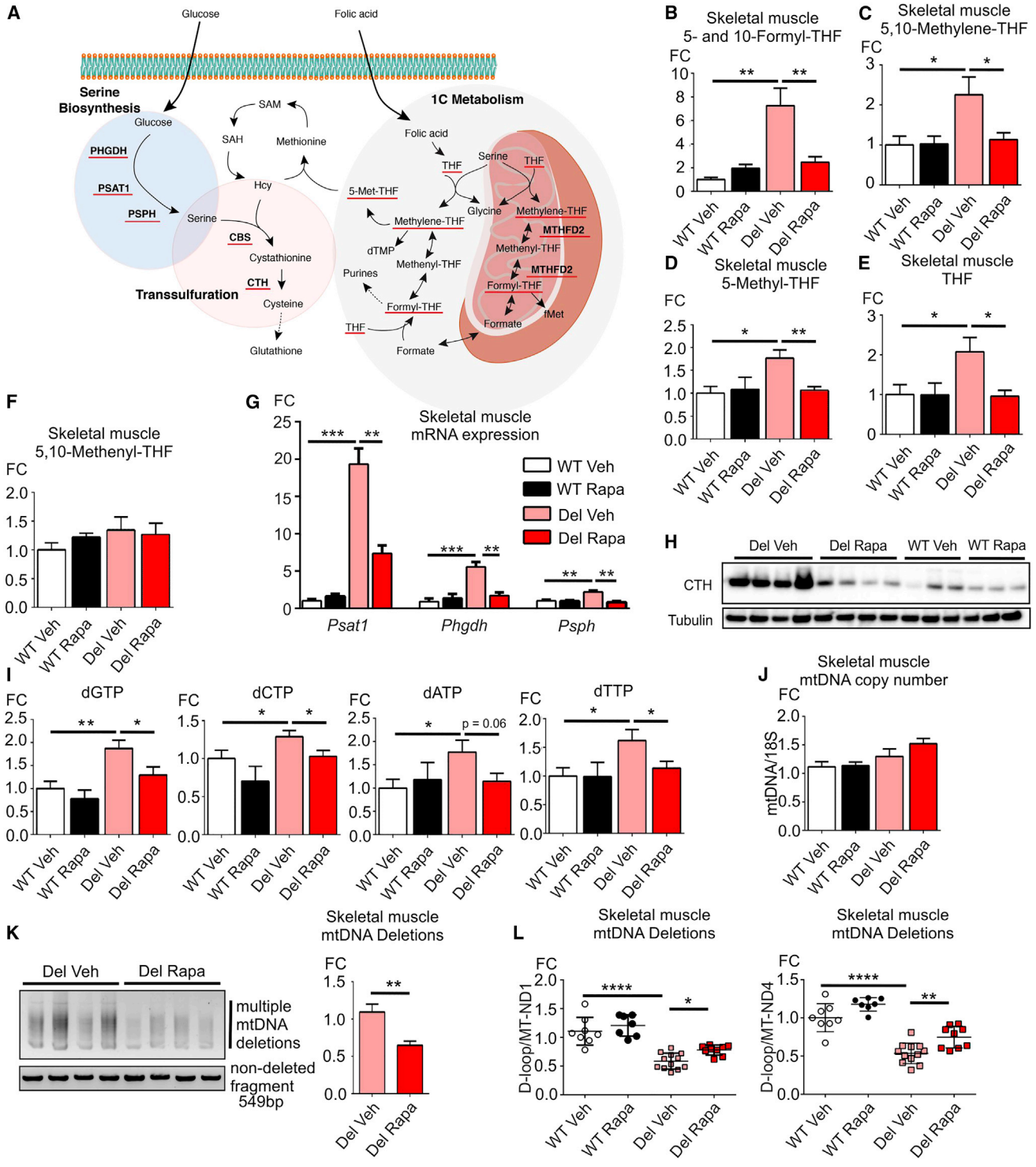

Figure 2. mTORC1 Regulates 1C Metabolism and Serine Biosynthesis in MM

(A) Schematic representation of 1C metabolism, serine biosynthesis, and transsulfuration pathways. Underlined metabolites and proteins were downregulated after mTORC1 inhibition by rapa.

(B–F) Tetrahydrofolate (THF) intermediate concentrations in skeletal muscle (B, 5- and 10-formyl-THF; C, 5,10-methylene-THF; D, 5-methyl-THF; E, THF; and F, 5,10-methenyl-THF; WT vehicle, n = 5; WT rapa, n = 5; Deletor vehicle, n = 6; Deletor rapa, n = 6) by ultra-performance liquid chromatography-tandem mass spectrometry (UPLC-MS/MS) analysis of tissue extracts.

(G) Enzymes of serine de novo biosynthesis, mRNA expression levels in skeletal muscle: *Psat1*, *Phgdh*, and *Psph* (WT vehicle, n = 7; WT rapa, n = 7; Deletor vehicle, n = 9; Deletor rapa, n = 9).

(legend continued on next page)

The evidence suggests that mTORC1 regulates both AARE response and UPRmt in MM-related stress response.

Rapamycin Balances 1C Metabolism, De Novo Serine Biosynthesis, and Transsulfuration in MM

The induction of mitochondrial folate cycle in MM results in wide remodeling of metabolism, in particular anabolic 1C-dependent biosynthetic pathways and de novo serine biosynthesis, which in Deletor muscle is the main direction of glucose flux (Bao et al., 2016; Locasale et al., 2011; Nikkanen et al., 2016). In folate cycle, different tetrahydrofolate forms carry 1C units to specific biosynthetic enzymes in, e.g., methyl cycle, purine, and dTMP synthesis (Figure 2A). The imbalanced folate cycle intermediates in Deletor muscle were rescued to WT level by rapa (Figures 2B–2F). Also, the expression levels of the three enzymes of de novo serine synthesis, phosphoserine aminotransferase, phosphoglycerate hydrogenase, and phosphoserine phosphatase were decreased (Figure 2G). Serine is also required in the transsulfuration pathway that produces cysteine for glutathione and taurine synthesis (Figure 2A). The rate-limiting enzymes, cystathionine beta synthase and cystathionine gamma lyase, were increased in Deletor muscle and completely rescued to WT level by rapa (Figures 2H and S1D). Furthermore, the imbalanced, genotoxic dNTP pools of Deletor muscle, suggested to contribute to multiple mtDNA deletion formation in MM (Nikkanen et al., 2016), were corrected to WT level by rapa (Figure 2I). The steady-state mtDNA amount was unaffected, but mtDNA deletion load was significantly decreased, suggesting decreased pathology (Figures 2J–2L).

These data suggest that mTORC1 coordinates induction of 1C-dependent anabolic biosynthesis pathways in MM, including folate cycle, de novo serine biosynthesis, transsulfuration, and dNTP synthesis.

Rapamycin Remodels Muscle Metabolome

The global muscle metabolomes of WT and Deletor mice clustered separately in unsupervised analysis, but overlapped after rapa treatment (Figure 3A). This finding indicates the considerable remodeling effects of rapa to muscle metabolism and highlights the global change of MM metabolism toward WT. In Deletors, intermediates of nucleotide metabolism (e.g., IMP, cytidine, and deoxycytidine) and most acyl-carnitines became WT-like after rapa administration (Figures 3B and 3C). mTORC1 inhibition resulted in an overall lowered abundance of free metabolites, consistent with decreased biosynthesis (Figure 3B). Glutamine and arginine, both known inducers of mTORC1, were increased in all rapa-treated mice, consistent with their metabolic feedback regulation with mTORC1 in skeletal muscle (Figure 3B).

The results indicate the power of targeted quantitative metabolomics and clustering analysis as a tool to follow treatment effect in therapy trials. Furthermore, the data indicate that even in advanced disease of Deletors, the pathologic metabolic signature is reversible.

Increased Macroautophagy in Rapamycin-Treated Deletors

The decrease of mtDNA deletion amount could be explained by decreased deletion generation, increased turnover of muscle mtDNAs, or turnover of the whole organelles. mTORC1 activity suppresses autophagy, resulting in accumulation of polyubiquitinated cargo and its receptor SQSTM1 (p62) (Bjørkøy et al., 2006, 2009; Kim et al., 2011; Kundu, 2011). In Deletor muscle, steady-state SQSTM1 was increased, as was slightly the polymerized autophagic membrane components LC3-II and phosphatidylethanolamine, suggesting stalled autophagy (Figures 3D and 3E). Rapa treatment rescued these macroautophagy components to WT level (Figures 3D and 3E).

Inhibition of mTORC1 Decreases mtDNA Mutagenesis and RRF Amounts in MM

As rapa effectively suppressed disease-related transcriptomic and metabolomic responses, we asked whether it also affected MM progression and its typical morphological signs. COX-negative muscle fibers were decreased 2-fold, and SDH-positive RRFs 4-fold (Figures 4A, 4B, and S2A), consistent with decreased mtDNA deletion load. Rapa did not only halt the progression of disease, but also showed a curative effect: the treated 24-month-old mice had ~3-fold fewer RRFs than Deletors at 22 months at treatment initiation (Figure 4B). Rapa did not affect muscle fiber size (Figure S2B). Electron microscopic analysis indicated that rapa-treated Deletor mice had improved muscle ultrastructure, with fewer abnormal crista formations, improved crista density, and enlarged hypodense mitochondria compared to untreated mice (Figures 4C and 4E). The treatment did not affect muscle RC enzyme protein amounts or expression levels of *Pgc1-a*, its target *Err-a*, or enzymes related to fatty acid uptake or beta-oxidation, oxygen utilization, CO_2 production, or respiratory exchange ratio (Figures S2C–S2F), indicating that mitochondrial biogenesis was not induced. The Deletors do not have muscle weakness, and their grip strength was WT-like before and after rapa treatment (Figure S3A), indicating that suppressing stress responses did not compromise muscle strength.

(H) Expression of CTH in skeletal muscle by western blot.

(I) dNTP concentrations in skeletal muscle (WT vehicle, n = 8; WT rapa, n = 7; Deletor vehicle, n = 10; Deletor rapa, n = 8).

(J) mtDNA copy number in skeletal muscle. qPCR analysis using 18S gene as a nuclear two-copy control gene (WT vehicle, n = 7; WT rapa, n = 7; Deletor vehicle, n = 9; Deletor rapa, n = 9).

(K) Multiple mtDNA deletions in skeletal muscle. Smear: deleted mtDNA species in long-range PCR amplification. Non-deleted 549 bp mtDNA fragment, product from 12S rRNA gene in mtDNA, represents total mtDNA amount (Deletor vehicle, n = 9; Deletor rapa, n = 9).

(L) mtDNA deletion quantification using triplex qPCR. D-loop/ND1 (left) and D-loop/ND4 (right) (WT vehicle, n = 8; WT rapa, n = 7; Deletor vehicle, n = 12; Deletor rapa, n = 8).

All data are shown as mean with SEM. Statistical testing was done by using Student's t test; *$p \leq 0.05$, **$p \leq 0.01$, ***$p \leq 0.001$, ****$p \leq 0.0001$. FC, fold change; Hcy, homocysteine; SAH, S-adenosyl-homocysteine; SAM, S-adenosyl-methionine; dTMP, thymidine monophosphate; fMet, formylmethionine; THF, tetrahydrofolate; 1C, one-carbon.

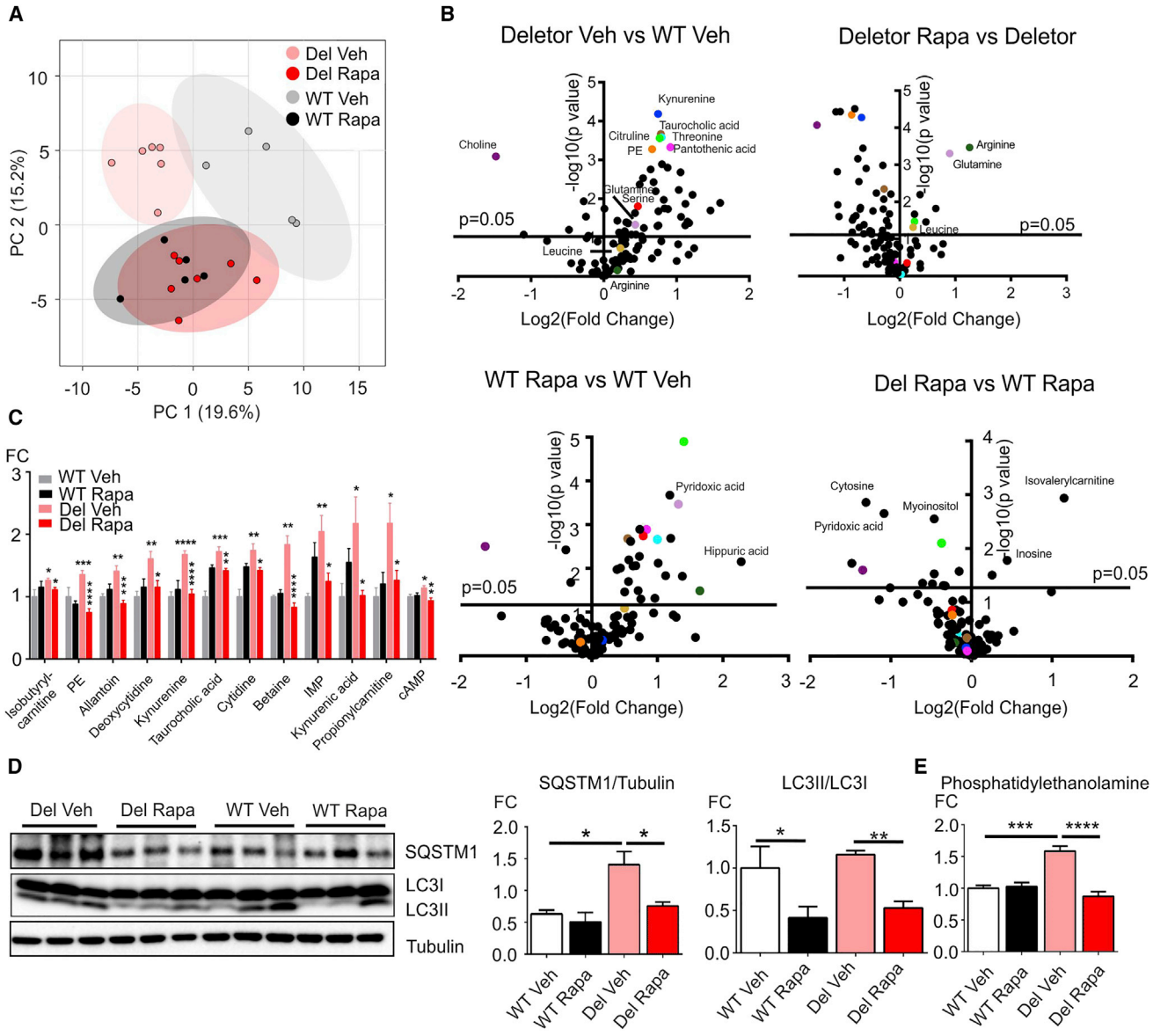

Figure 3. Disease-Associated Metabolic Profile Rescued by mTORC1 Inhibition

(A) Principal component analysis (PCA) of metabolomic data in skeletal muscle of WT and Deletor mice treated with vehicle or rapa.

(B) Metabolomic changes in mitochondrial disease and WT mice before and after rapa treatment. Volcano plots of analyzed metabolites. Colors indicate the most significantly changed metabolites in Deletors compared to WT mice, and their levels in all plots.

(C) Metabolites increased in Deletors, affected by rapa treatment. Asterisks above Deletor vehicle bars indicate comparison to WT vehicle. Asterisks above Deletor rapa bars indicate comparison to Deletor vehicle.

(D) Macroautophagy in MM. Expression of SQSTM1 and LC3 in skeletal muscle (LC3I soluble form and LC3II membrane-associated form) and quantification of signals.

(E) Phosphatidylethanolamine in skeletal muscle.

All data are shown as mean with SEM. Statistical testing was done by using Student's t test; *p ≤ 0.05, **p ≤ 0.01, ***p ≤ 0.001, ****p ≤ 0.0001.

These findings indicate that mTORC1 activation promotes the progression of MM and that rapa can partially reverse the disease process, even at advanced disease stage.

Cardiac Septum Hypertrophy Improved by mTORC1 Inhibition

Other affected organs in the Deletor are the heart and brown adipose tissue (BAT). The robust induction of AARE genes and de novo serine biosynthesis in the heart were suppressed by rapa, similar to skeletal muscle (Figures S3B–S3E). Our echocardiographic analysis showed that rapa treatment decreased left ventricular mass in both WT and Deletors, but did not affect the functional parameters (Figure S3F). Deletors showed a tendency to slight hypertrophy of the interventricular septum in both systole and diastole, a typical sign in some mitochondrial disease patients, increasing their risk of arrhythmia

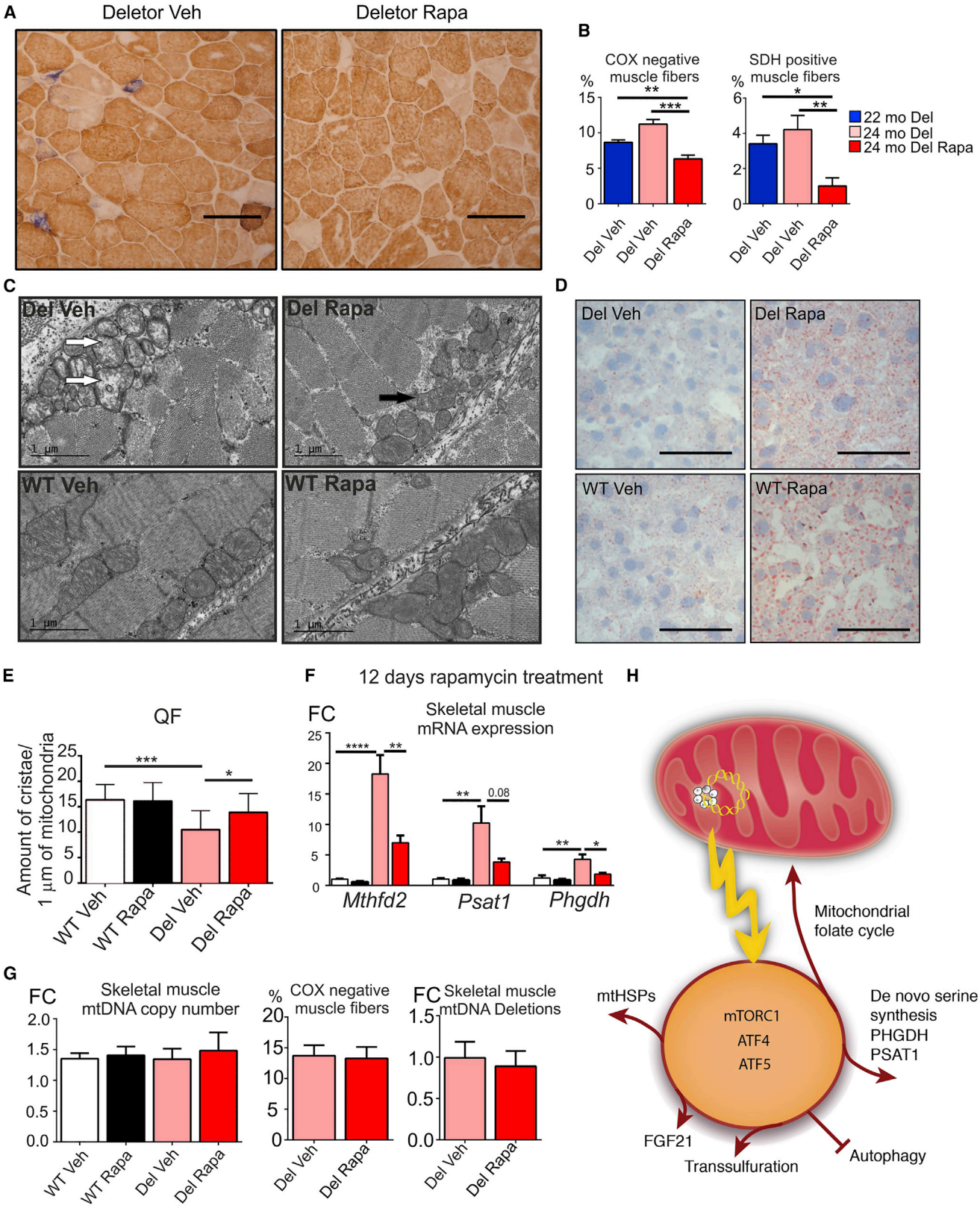

(legend on next page)

complications (Heliö et al., 2013). Rapa cured this septum hypertrophy (Figure S3F).

The liver lipid content increased after rapa both in WT and Deletors (Figure 4D). In BAT, lipid droplets also increased in size, but rapa did not significantly rescue the ultrastructural changes such as crista density to WT level (Figures S4A–S4C), suggesting some tissue specificity of mTORC1 roles in mitochondrial disease.

mTORC1 Is Directly Upstream of Integrated Mitochondrial Stress Response

Our results demonstrated that mTORC1 is activated by primary MM, and that its inhibition rescues disease markers and stress responses. However, whether the rescue of responses was directly linked to mTORC1 or was a consequence of improved muscle health remained unclear. We treated the mice with rapamycin for 12 days, which resulted in decreased expression of *Mthfd2* and serine biosynthetic enzymes in Deletors (Figure 4F). However, RC-deficient fibers, mtDNA deletions, and total mtDNA amount remained unchanged (Figure 4G), pointing to the conclusion that mTORC1 is the upstream overall regulator of MM-related stress responses (Figure 4H).

In conclusion, our data indicate that mTORC1 is activated in MM muscle in a mosaic manner, correlates with severity of RC defect, and is the overarching inducer of an integrated mitochondrial stress response (ISRmt). This includes (1) ATF4-directed AARE response driving mitochondrial folate cycle, serine biosynthesis, and secretion of FGF21 cytokine (Bao et al., 2016; Nikkanen et al., 2016; Suomalainen et al., 2011; Tyynismaa et al., 2010); (2) mitochondrial UPRmt (Haynes et al., 2013); and (3) remodeling of 1C cycle with induced purine and glutathione synthesis and genotoxic dNTP pools (Nikkanen et al., 2016). Recent evidence in cultured cells suggested that mTORC1-activated ATF4 controls mitochondrial folate cycle and purine synthesis (Ben-Sahra et al., 2016), which we here show to be true in postmitotic tissues and contribute in disease progression. We propose that the AARE/ATF/UPRmt/folate-cycle responses are all part of ISRmt, and that FGF21 is the secreted signal of ISRmt. Previous literature proposed UPRmt to promote longevity and improved health (Houtkooper et al., 2013). Our data show that chronic induction in the context of MM, however, is not protective in pathogenesis.

Rapa has previously been reported to restore ATP levels in neurons with RC dysfunction (Zheng et al., 2016), but unlike other treatments improving mitochondrial health, we did not find it to induce mitochondrial biogenesis. PPAR or AMPK agonists, ketogenic diet, NAD precursors, and PARP inhibitors all activate sirtuins, AMPK, and beta-oxidation and increase mitochondrial mass and oxidative activity(Ahola et al., 2016; Ahola-Erkkilä et al., 2010; Cantó et al., 2012; Cerutti et al., 2014; Khan et al., 2014). AMPK inhibits mTOR, and therefore rapa and mitochondrial biogenesis inducers both inhibit anabolic metabolism, by a different mechanism. These data propose that chronic induction of anabolism is a key contributor for MM pathogenesis.

Serum FGF21 is an established biomarker for mtDNA deletion and translation diseases (Lehtonen et al., 2016; Suomalainen et al., 2011). We show that muscle FGF21 induction is under mTORC1 control in MM, the most common mitochondrial disease of adults. Our data suggest rapa treatment trials for adult MM patients who show increased serum FGF21.

STAR★METHODS

Detailed methods are provided in the online version of this paper and include the following:

- KEY RESOURCES TABLE
- CONTACT FOR REAGENT AND RESOURCE SHARING
- EXPERIMENTAL MODEL AND SUBJECT DETAILS
  - Mouse Model
  - Cell Lines
- METHOD DETAILS
  - Rapamycin Administration
  - Mouse Phenotyping and Grip Strength
  - Analysis of Whole-Body Metabolism
  - Cardiac Echocardiography
  - Morphological Analysis
  - Serum FGF21 Measurement
  - mtDNA Deletion Analyses
  - mtDNA Copy Number Analysis
  - ATF4 Silencing Experiments
  - Western Blotting
  - Gene Expression

Figure 4. Inhibition of mTORC1 Ameliorates Disease Pathogenesis

(A) Rapa effect on RC activities in Deletor muscle. Histochemical analysis of cytochrome *c* oxidase (COX; brown) and succinate dehydrogenase (SDH; blue) activities. Scale bars, 100 μm.

(B) COX-negative and SDH-positive muscle fibers before treatment (blue bars) and after vehicle versus rapa treatment (Deletor vehicle, 24 months, n = 9; Deletor rapa, 24 months, n = 9; Deletor, 22 months, n = 8).

(C) Electron micrograph of Deletor and WT muscle. Deletor vehicle, arrows indicate abnormal mitochondria; Deletor rapa, white arrow indicates abnormal mitochondrion; black arrow indicates normal mitochondrion. Scale bar, 1 μm.

(D) Liver fat content, stained by Oil Red O in frozen sections. Red, lipid (hematoxylin counterstaining). Scale bars, 100 μm.

(E) Mitochondrial crista density, quantified from quadriceps femoris muscle (QF). Image analysis (WT vehicle, n = 3; WT rapa, n = 3; Deletor vehicle, n = 3; Deletor rapa, n = 3).

(F) Twelve days of rapa treatment: *Mthfd2, Psat1*, and *Phgdh* mRNA levels in skeletal muscle (WT vehicle, n = 6; WT rapa, n = 6; Deletor vehicle, n = 6; Deletor rapa, n = 5).

(G) Quantification of mtDNA copy number, RC-deficient muscle fibers, and mtDNA deletion load (WT vehicle, n = 6; WT rapa, n = 6; Deletor vehicle, n = 6; Deletor rapa, n = 5).

(H) Schematic representation of ISRmt in mitochondrial disease, controlled by mTORC1.

All data are shown as mean with SEM. Statistical testing was done by using Student's t test; *$p \leq 0.05$, **$p \leq 0.01$, ***$p \leq 0.001$, ****$p \leq 0.0001$.

See also Figure S4.

- Metabolomics Data Analysis
- dNTP Pool Measurement

- QUANTIFICATION AND STATISTICAL ANALYSIS

SUPPLEMENTAL INFORMATION

Supplemental Information includes four figures and one table and can be found with this article online at http://dx.doi.org/10.1016/j.cmet.2017.07.007.

AUTHOR CONTRIBUTIONS

N.A.K. was in charge of study experimentation and design, data analysis, and writing of the first manuscript draft. J.N., S.Y., and C.J. designed and did experiments and analyzed and interpreted data; L.W. analyzed dNTP pools; S.P. performed and analyzed actinonin experiments; R.K. was the expert of echocardiography; V.V. and A.P. performed metabolomics analysis and interpreted results; and A.S. supervised the project, conceived the study, and analyzed and interpreted data. All authors contributed to manuscript writing and commenting.

ACKNOWLEDGMENTS

The authors wish to thank Anu Harju, Markus Innilä, Tuula Manninen, and Jatin Nandania for technical help; Henna Tyynismaa, Emil Ylikallio, Alexandra Götz, and Sofia Ahola for useful scientific discussions and expertise; Electron Microscopy Core Facility of Helsinki University for expertise in ultrastructural experiments; and the Helsinki University Laboratory Animal Centre for excellent maintenance of the animals. We also acknowledge the following funding sources: United Mitochondrial Disease Foundation, Jane and Aatos Erkko Foundation, Sigrid Jusélius Foundation, Academy of Finland, University of Helsinki, European Research Council (ERC-AdG10-268955) (for A.S.), Helsinki Biomedical Graduate School (for J.N.) and Swiss National Foundation, and the Novartis Foundation for medical biological research (for C.J.).

Received: December 1, 2016
Revised: May 15, 2017
Accepted: July 14, 2017
Published: August 1, 2017

REFERENCES

Ahola, S., Auranen, M., Isohanni, P., Niemisalo, S., Urho, N., Buzkova, J., Velagapudi, V., Lundbom, N., Hakkarainen, A., Muurinen, T., et al. (2016). Modified Atkins diet induces subacute selective ragged-red-fiber lysis in mitochondrial myopathy patients. EMBO Mol. Med. *8*, 1234–1247.

Ahola-Erkkilä, S., Carroll, C.J., Peltola-Mjösund, K., Tulkki, V., Mattila, I., Seppänen-Laakso, T., Oresic, M., Tyynismaa, H., and Suomalainen, A. (2010). Ketogenic diet slows down mitochondrial myopathy progression in mice. Hum. Mol. Genet. *19*, 1974–1984.

Bao, X.R., Ong, S.E., Goldberger, O., Peng, J., Sharma, R., Thompson, D.A., Vafai, S.B., Cox, A.G., Marutani, E., Ichinose, F., et al. (2016). Mitochondrial dysfunction remodels one-carbon metabolism in human cells. Elife *5*, http://dx.doi.org/10.7554/eLife.10575.

Ben-Sahra, I., Hoxhaj, G., Ricoult, S.J., Asara, J.M., and Manning, B.D. (2016). mTORC1 induces purine synthesis through control of the mitochondrial tetrahydrofolate cycle. Science *351*, 728–733.

Bjørkøy, G., Lamark, T., and Johansen, T. (2006). p62/SQSTM1: a missing link between protein aggregates and the autophagy machinery. Autophagy *2*, 138–139.

Bjørkøy, G., Lamark, T., Pankiv, S., Øvervatn, A., Brech, A., and Johansen, T. (2009). Monitoring autophagic degradation of p62/SQSTM1. Methods Enzymol. *452*, 181–197.

Cantó, C., Houtkooper, R.H., Pirinen, E., Youn, D.Y., Oosterveer, M.H., Cen, Y., Fernandez-Marcos, P.J., Yamamoto, H., Andreux, P.A., Cettour-Rose, P., et al. (2012). The NAD(+) precursor nicotinamide riboside enhances oxidative metabolism and protects against high-fat diet-induced obesity. Cell Metab. *15*, 838–847.

Cerutti, R., Pirinen, E., Lamperti, C., Marchet, S., Sauve, A.A., Li, W., Leoni, V., Schon, E.A., Dantzer, F., Auwerx, J., et al. (2014). NAD(+)-dependent activation of Sirt1 corrects the phenotype in a mouse model of mitochondrial disease. Cell Metab. *19*, 1042–1049.

Chen, J., Zheng, X.F., Brown, E.J., and Schreiber, S.L. (1995). Identification of an 11-kDa FKBP12-rapamycin-binding domain within the 289-kDa FKBP12-rapamycin-associated protein and characterization of a critical serine residue. Proc. Natl. Acad. Sci. USA *92*, 4947–4951.

Chinnery, P.F. (2015). Mitochondrial disease in adults: what's old and what's new? EMBO Mol. Med. *7*, 1503–1512.

Christensen, K.E., and MacKenzie, R.E. (2006). Mitochondrial one-carbon metabolism is adapted to the specific needs of yeast, plants and mammals. BioEssays *28*, 595–605.

Haynes, C.M., Petrova, K., Benedetti, C., Yang, Y., and Ron, D. (2007). ClpP mediates activation of a mitochondrial unfolded protein response in C. elegans. Dev. Cell *13*, 467–480.

Haynes, C.M., Fiorese, C.J., and Lin, Y.F. (2013). Evaluating and responding to mitochondrial dysfunction: the mitochondrial unfolded-protein response and beyond. Trends Cell Biol. *23*, 311–318.

Heliö, T.M., Götz, A., Rapola, J., Kiuru-Enari, S., Kivistö, S., Heikinheimo, T., and Suomalainen, A. (2013). Atrial fibrillation is poorly tolerated by patients with hypertrophic concentric cardiomyopathy caused by mitochondrial tRNALeu (UUR) mutations. Cardiogenetics *3*, e6.

Houtkooper, R.H., Mouchiroud, L., Ryu, D., Moullan, N., Katsyuba, E., Knott, G., Williams, R.W., and Auwerx, J. (2013). Mitonuclear protein imbalance as a conserved longevity mechanism. Nature *497*, 451–457.

Jain, M., Nilsson, R., Sharma, S., Madhusudhan, N., Kitami, T., Souza, A.L., Kafri, R., Kirschner, M.W., Clish, C.B., and Mootha, V.K. (2012). Metabolite profiling identifies a key role for glycine in rapid cancer cell proliferation. Science *336*, 1040–1044.

Johnson, S.C., Yanos, M.E., Kayser, E.B., Quintana, A., Sangesland, M., Castanza, A., Uhde, L., Hui, J., Wall, V.Z., Gagnidze, A., et al. (2013). mTOR inhibition alleviates mitochondrial disease in a mouse model of Leigh syndrome. Science *342*, 1524–1528.

Khan, N.A., Auranen, M., Paetau, I., Pirinen, E., Euro, L., Forsström, S., Pasila, L., Velagapudi, V., Carroll, C.J., Auwerx, J., and Suomalainen, A. (2014). Effective treatment of mitochondrial myopathy by nicotinamide riboside, a vitamin B3. EMBO Mol. Med. *6*, 721–731.

Kim, J., Kundu, M., Viollet, B., and Guan, K.L. (2011). AMPK and mTOR regulate autophagy through direct phosphorylation of Ulk1. Nat. Cell Biol. *13*, 132–141.

Koopman, W.J., Beyrath, J., Fung, C.W., Koene, S., Rodenburg, R.J., Willems, P.H., and Smeitink, J.A. (2016). Mitochondrial disorders in children: toward development of small-molecule treatment strategies. EMBO Mol. Med. *8*, 311–327.

Kundu, M. (2011). ULK1, mammalian target of rapamycin, and mitochondria: linking nutrient availability and autophagy. Antioxid. Redox Signal. *14*, 1953–1958.

Lehtonen, J.M., Forsström, S., Bottani, E., Viscomi, C., Baris, O.R., Isoniemi, H., Höckerstedt, K., Österlund, P., Hurme, M., Jylhävä, J., et al. (2016). FGF21 is a biomarker for mitochondrial translation and mtDNA maintenance disorders. Neurology *87*, 2290–2299.

Locasale, J.W., Grassian, A.R., Melman, T., Lyssiotis, C.A., Mattaini, K.R., Bass, A.J., Heffron, G., Metallo, C.M., Muranen, T., Sharfi, H., et al. (2011). Phosphoglycerate dehydrogenase diverts glycolytic flux and contributes to oncogenesis. Nat. Genet. *43*, 869–874.

Ma, X.M., and Blenis, J. (2009). Molecular mechanisms of mTOR-mediated translational control. Nat. Rev. Mol. Cell Biol. *10*, 307–318.

Nargund, A.M., Pellegrino, M.W., Fiorese, C.J., Baker, B.M., and Haynes, C.M. (2012). Mitochondrial import efficiency of ATFS-1 regulates mitochondrial UPR activation. Science *337*, 587–590.

Nikkanen, J., Forsström, S., Euro, L., Paetau, I., Kohnz, R.A., Wang, L., Chilov, D., Viinamäki, J., Roivainen, A., Marjamäki, P., et al. (2016). Mitochondrial DNA replication defects disturb cellular dNTP pools and remodel one-carbon metabolism. Cell Metab. *23*, 635–648.

Nilsson, R., Jain, M., Madhusudhan, N., Sheppard, N.G., Strittmatter, L., Kampf, C., Huang, J., Asplund, A., and Mootha, V.K. (2014). Metabolic enzyme expression highlights a key role for MTHFD2 and the mitochondrial folate pathway in cancer. Nat. Commun. *5*, 3128.

Olson, W., Engel, W.K., Walsh, G.O., and Einaugler, R. (1972). Oculocraniosomatic neuromuscular disease with "ragged-red" fibers. Arch. Neurol. *26*, 193–211.

Richter, U., Lahtinen, T., Marttinen, P., Suomi, F., and Battersby, B.J. (2015). Quality control of mitochondrial protein synthesis is required for membrane integrity and cell fitness. J. Cell Biol. *211*, 373–389.

Rygiel, K.A., Grady, J.P., Taylor, R.W., Tuppen, H.A., and Turnbull, D.M. (2015). Triplex real-time PCR—an improved method to detect a wide spectrum of mitochondrial DNA deletions in single cells. Sci. Rep. *5*, 9906.

Sabatini, D.M., Erdjument-Bromage, H., Lui, M., Tempst, P., and Snyder, S.H. (1994). RAFT1: a mammalian protein that binds to FKBP12 in a rapamycin-dependent fashion and is homologous to yeast TORs. Cell *78*, 35–43.

Saxton, R.A., and Sabatini, D.M. (2017). mTOR signaling in growth, metabolism, and disease. Cell *169*, 361–371.

Shimobayashi, M., and Hall, M.N. (2014). Making new contacts: the mTOR network in metabolism and signalling crosstalk. Nat. Rev. Mol. Cell Biol. *15*, 155–162.

Shoubridge, E.A., Johns, T., and Boulet, L. (1996). Use of myoblast cultures to study mitochondrial myopathies. Methods Enzymol. *264*, 465–475.

Spelbrink, J.N., Li, F.Y., Tiranti, V., Nikali, K., Yuan, Q.P., Tariq, M., Wanrooij, S., Garrido, N., Comi, G., Morandi, L., et al. (2001). Human mitochondrial DNA deletions associated with mutations in the gene encoding Twinkle, a phage T7 gene 4-like protein localized in mitochondria. Nat. Genet. *28*, 223–231.

Suomalainen, A., Majander, A., Haltia, M., Somer, H., Lönnqvist, J., Savontaus, M.L., and Peltonen, L. (1992). Multiple deletions of mitochondrial DNA in several tissues of a patient with severe retarded depression and familial progressive external ophthalmoplegia. J. Clin. Invest. *90*, 61–66.

Suomalainen, A., Elo, J.M., Pietiläinen, K.H., Hakonen, A.H., Sevastianova, K., Korpela, M., Isohanni, P., Marjavaara, S.K., Tyni, T., Kiuru-Enari, S., et al. (2011). FGF-21 as a biomarker for muscle-manifesting mitochondrial respiratory chain deficiencies: a diagnostic study. Lancet Neurol. *10*, 806–818.

Taylor, R.C., Berendzen, K.M., and Dillin, A. (2014). Systemic stress signalling: understanding the cell non-autonomous control of proteostasis. Nat. Rev. Mol. Cell Biol. *15*, 211–217.

Tyynismaa, H., Mjosund, K.P., Wanrooij, S., Lappalainen, I., Ylikallio, E., Jalanko, A., Spelbrink, J.N., Paetau, A., and Suomalainen, A. (2005). Mutant mitochondrial helicase Twinkle causes multiple mtDNA deletions and a late-onset mitochondrial disease in mice. Proc. Natl. Acad. Sci. USA *102*, 17687–17692.

Tyynismaa, H., Carroll, C.J., Raimundo, N., Ahola-Erkkilä, S., Wenz, T., Ruhanen, H., Guse, K., Hemminki, A., Peltola-Mjøsund, K.E., Tulkki, V., et al. (2010). Mitochondrial myopathy induces a starvation-like response. Hum. Mol. Genet. *19*, 3948–3958.

Xia, J., Psychogios, N., Young, N., and Wishart, D.S. (2009). MetaboAnalyst: a web server for metabolomic data analysis and interpretation. Nucleic Acids Res. *37*, W652–W660.

Yatsuga, S., and Suomalainen, A. (2012). Effect of bezafibrate treatment on late-onset mitochondrial myopathy in mice. Hum. Mol. Genet. *21*, 526–535.

Yatsuga, S., Fujita, Y., Ishii, A., Fukumoto, Y., Arahata, H., Kakuma, T., Kojima, T., Ito, M., Tanaka, M., Saiki, R., and Koga, Y. (2015). Growth differentiation factor 15 as a useful biomarker for mitochondrial disorders. Ann. Neurol. *78*, 814–823.

Young, M.J., and Copeland, W.C. (2016). Human mitochondrial DNA replication machinery and disease. Curr. Opin. Genet. Dev. *38*, 52–62.

Zheng, X., Boyer, L., Jin, M., Kim, Y., Fan, W., Bardy, C., Berggren, T., Evans, R.M., Gage, F.H., and Hunter, T. (2016). Alleviation of neuronal energy deficiency by mTOR inhibition as a treatment for mitochondria-related neurodegeneration. Elife *5*, http://dx.doi.org/10.7554/eLife.13378.

STAR★METHODS

KEY RESOURCES TABLE

REAGENT or RESOURCE	SOURCE	IDENTIFIER
Antibodies		
Rabbit anti-phospho-S6k	Cell Signaling Technology	Cat#9205
Rabbit anti-total-S6k	Cell Signaling Technology	Cat#9202
Rabbit anti-phospho-S6	Cell Signaling Technology	Cat#4858
Rabbit anti-total-S6	Cell Signaling Technology	Cat#2217
Rabbit anti-total-Akt	Cell Signaling Technology	Cat#4685
Rabbit anti-phospho-Akt (Thr450)	Cell Signaling Technology	Cat#9267
Rabbit anti-phospho-Akt (Thr308)	Cell Signaling Technology	Cat#2965
Rabbit anti-phospho-Akt (Thr473)	Cell Signaling Technology	Cat#4060
Rabbit anti-MTHFD2	Proteintech	Cat#12270-1-AP
Rabbit anti-CTH	Proteintech	Cat#12217-1-AP
Goat anti-HSP60	Santa Cruz Biotechnology	Cat#sc-1052
Rabbit anti-HSP70	Abcam	Cat#53098
Rabbit anti-CLPP	Proteintech	Cat#15698-1-AP
Rabbit anti-LONP1	Sigma Aldrich	Cat# HPA002192
Mouse anti-alpha Tubulin	Santa Cruz Biotechnology	Cat#sc-5286
Rabbit anti-SQSTM1/p62	Cell Signaling Technology	Cat#5114
Rabbit anti-LC3B	Abcam	Cat#ab168831
Rabbit anti-GAPDH	Cell Signaling Technology	Cat#2118
Rabbit anti-Porin	Abcam	Cat#ab15895
Rabbit anti-Tom20	Santa Cruz Biotechnology	Cat#sc-11415
Total OXPHOS rodent western blot cocktail	Abcam	Cat#110413
Goat anti-mouse IgG	Jackson ImmunoResearch	Cat#115-035-146
Goat anti-rabbit IgG	Jackson ImmunoResearch	Cat#111-035-144
Rabbit anti-goat IgG	Calbiochem	Cat#401504
Chemicals, Peptides, and Recombinant Proteins		
Rapamycin	LC Laboratories	Cat#R-5000
DMSO	Sigma Aldrich	Cat#D8418
PEG-400	Sigma Aldrich	Cat#202398
Phosphatase inhibitor cocktail	Thermo Scientific	Cat#78420
SYBR Green Supermix	Bio-Rad	Cat#1725006CUST
Protein assay kit	Bio-Rad	Cat#500-0114
Pierce Protease Inhibitor Mini Tablets, EDTA-Free	Thermo Scientific	Cat#88666
Actinonin	Sigma Aldrich	Cat#A6671
JET Prime transfection reagent	Polypus	Cat#114-07
TaqMan Universal PCR master mix	Applied Biosystems	Cat#4304437
Uridine	Calbiochem	Cat#6680
Dexamethasone	Sigma Aldrich	Cat#D1756
Insulin	Sigma Aldrich	Cat#I-1882
Fetuin	Sigma Aldrich	Cat#F-2379
Phusion High-Fidelity DNA Polymerase	Thermo Scientific	Cat#530L
Oil Red O	Sigma Aldrich	Cat#O0625
Glutaraldehyde solution	Sigma Aldrich	Cat#G7651
TRIzol Reagent	Thermo Scientific	Cat#15596026
Maxima First Strand cDNA Synthesis Kit for RT-qPCR	Thermo Scientific	Cat#K1671

(*Continued on next page*)

Continued		
REAGENT or RESOURCE	SOURCE	IDENTIFIER
Formic Acid	VWR CHEMICALS, Finland	Cat#84865.290
Acetonitrile	VWR CHEMICALS, Finland	Cat#1.59014.2500
Ascorbic Acid	Sigma Aldrich	Cat#A0278
HEPES	Sigma Aldrich	Cat#H3375
Critical Commercial Assays		
Mouse/Rat FGF-21 Quantikine ELISA Kit	R&D Systems	Cat#MF2100
Experimental Models: Cell Lines		
Human diploid male control myoblast cell line (established in-lab)	This study	N/A
Experimental Models: Organisms/Strains		
Tg/ACTB/twnk-p.353-365-dup/BL6	Suomalainen Lab	N/A
Oligonucleotides		
See Table S1 for primer sequences	This paper	N/A
Software and Algorithms		
ImageJ software	NIH	N/A
Prism 6 software (GraphPad Software)	GraphPad	N/A
Other		
Mouse diet	Altromin Spezialfutter	Cat#C1000

CONTACT FOR REAGENT AND RESOURCE SHARING

More information and requests for resources and reagents should be directed to and will be fulfilled by the Lead Contact, Anu Suomalainen Wartiovaara (anu.wartiovaara@helsinki.fi).

EXPERIMENTAL MODEL AND SUBJECT DETAILS

Mouse Model

The mouse model used in this study (Deletor) was generated in C57BL/6 congenic background and carry a transgene with a dominant mutation (duplication of amino acids p.353-365) in *Twnk* encoding mitochondrial DNA helicase Twinkle and has been previously characterized (Tyynismaa et al., 2005); WT mice were littermates from the same congenic mouse strain C57BL/6. All the experiments were performed using 22-month-old male mice from two independent transgenic mouse lines (C and D), as described in Tyynismaa et al. (2005). Mice were housed in individual cages in controlled room at 22°C and 12h light/dark cycle with ad libitum access to food and water and were regularly monitored for weight and food consumption. All the mice in this study were given rodent diet with 11% fat, 65% carbohydrate, 24% protein of total calorie content, Altromin Spezialfutter GmbH & Co. KG, Germany.

The food intake in the long-term rapamycin treatment (70 days), group was controlled by removing the food from the cages 4 hr before mice were sacrificed for sample collection. In short term treatment (12 days), mice were fasted overnight, refed for two hours and sampled after 4 hr of fasting.

Animal experiments were performed according to guidelines approved by the ethical board of State province Office for Animal Experimentation of Finland.

Cell Lines

Primary myoblasts were isolated from a healthy 45-years-old male Caucasian donor as described before (Shoubridge et al., 1996). Myoblasts below passage 5 were used for experimental manipulations and grown in 420 mL Ham's F10 with GlutaMax (GIBCO 41550-021) supplemented with 75 mL of heat-inactivated FBS (Sigma, F9665), 250 mg BSA (Sigma #A-4503), 250 mg Fetuin (Sigma #F-2379), 90 mg Insulin (Sigma #I-1882), 5 mL of 39 μg / mL Dexamethasone (Sigma, #D1756), 500 μL Epidermal growth factor (10 μg/ml, BD Biosciences, 354052), 10 mg uridine (Calbiochem, 6680). Cells were maintained at 37°C at 5% CO_2.

METHOD DETAILS

Rapamycin Administration

Rapamycin (LC Laboratories #R-5000) was dissolved in DMSO to 100 mg/mL, and diluted in 5% PEG-400 to final concentration of 1.2 mg/mL, sterile filtered and stored at −80°C. Each mouse was weighed and the dose was adjusted to the final concentration of

8 mg/kg/day and injected intraperitoneally (i.p.) for 70 days. For short term treatment, similar dose of rapamycin was injected i.p. for 12 days. The control group was injected with vehicle containing the same volume of diluent and DMSO without rapamycin.

Mouse Phenotyping and Grip Strength

Body weights of all mice were measured during the whole study using a small electronic balance suitable for rodents. Grip strength was measured using the BIO-GS3 apparatus (Bioseb) by placing each animal on the platform until all the four limbs were engaged on the grid. Mice were then pulled until they released their grip to measure their muscle force. The mean of five measurements was normalized to body weight (g/g) for each animal tested. All animals were trained for three successive days before the actual experiment was performed.

Analysis of Whole-Body Metabolism

Oxymax Comprehensive Lab Animal Monitoring System (CLAMS; Columbus Instruments, OH, USA) was used to measure oxygen consumption and carbon dioxide production, as well as spontaneous moving and feeding activities. Mice were monitored using CLAMS 60 days after initiation of rapamycin injections. The mice were kept in individual cages in the CLAMS chambers for 3 days; the first day and night was a non-recording adjustment period followed by a 24-h recording at room temperature (+22°C). Measurements were performed for a total of 12 Deletor mice (n = 6 rapamycin-treated and n = 6 vehicle) and 12 WT mice (n = 6 on rapamycin and n = 6 vehicle). Respiratory exchange ratios were calculated as a ratio of CO_2 production and O_2 consumption, separately from the light (inactive) and dark (active) periods of the day.

Cardiac Echocardiography

Cardiac function was analyzed using a Vevo 2100 Ultrasound System (Visual Sonics, Toronto, ON, Canada). The animals were anesthetized with isoflurane for maximum of 15 min during the imaging (induction: 4.5% isoflurane, 450 ml/min air, maintenance: 1.5% isoflurane, 200 ml/min air, Baxter International, Deerfield, IL). Left ventricular mass, ejection fraction, fractional shortening, interventricular spectrum width (diastolic and systolic), left ventricular internal diameter (diastolic and systolic), left ventricular posterior wall width (diastolic and systolic) and left ventricular volume (diastolic and systolic) were determined from the parasternal short-axis (SAX) M-mode measurements. EF was calculated by the Vevo software using Teicholz formula.

Morphological Analysis

Samples from the *Quadriceps femoris* (QF) muscle, liver, heart and brown adipose tissue (BAT) were harvested immediately after sacrificing the mice, embedded in OCT Compound Embedding Medium (Tissue-Tek) and snap-frozen in 2-methylbutane bath in liquid nitrogen. In situ histochemical COX and SDH activities were analyzed from Frozen tissue sections (12 μm) from QF and heart (Tyynismaa et al., 2005). Approximately 2000 fibers from each mouse in the study group were counted to calculate the percentage of COX-negative and COX-negative/SDH-positive fibers from QF sections. The phospho-S6 amount (immunohistochemistry; Cell signaling, #4858) and COX-SDH activities were analyzed from consecutive QF sections. To analyze ragged red fibers, consecutive sections were stained with NADH tetrazolium reductase and Gomori Trichrome to visualize accumulations of mitochondria. Stained sections were analyzed by light microscopy (Axioplan 2 Universal Microscope, Zeiss). The quantification of COX-negative and SDH-positive fibers, pS6 and COX staining intensities, and muscle fiber sizes from each study group was performed using ImageJ software.

Fat content of frozen liver and BAT sections of 8 μm was assessed with Oil Red O staining. The slides were fixed in formic calcium (1:10:1 concentrated formalin: aqua: 10% calcium chloride) and then incubated in Oil Red O solution for 10 min. Oil Red O stock solution (1 mg/mL in isopropanol) was made by heating the reagent and alcohol at 56°C for 30 min. Fresh working solution was made from cooled stock solution and aqua (3:2). The working solution was properly mixed, filtered and used within few hours. The nuclei were stained with Mayer's hematoxylin (Ahola-Erkkilä et al., 2010). Stained sections were analyzed by light microscopy.

For plastic embedding, QF, heart, liver and BAT samples were fixed in 2.5% glutaraldehyde. They were then treated with 1% osmium tetroxide dehydrated in ethanol and embedded in epoxy resin. Sections (1 μm) were stained with methyl blue (0.5% w/v) and boric acid (1% w/v). The interesting areas for the ultrastructural analyses were selected by analyzing the sections with light microscope. For transmission electron microscopy, ultrathin (60–90 nm) sections were cut on grids and stained with uranyl acetate and lead citrate and viewed with JEOL 1400 Transmission Electron Microscopy (Khan et al., 2014). Crista density in mitochondria was measured by ImageJ software, using a "measuring stick" of 1 μm, placed perpendicular to the crista lamellae and cristae were counted over 20 μm of mitochondrial length.

Serum FGF21 Measurement

Blood samples were collected by heart puncture, and serum samples were prepared by centrifugation at 3000 x g for 15 min and stored at −80°C. Serum FGF-21 concentration was analyzed using Mouse/Rat FGF-21 Quantikine ELISA Kit from R&D systems as per manufacturer's instructions. Microplate was read by Spectra-Max 190 Absorbance Microplate Reader (Molecular Devices, USA) and analyzed by SoftMax Pro (Molecular Devices).

mtDNA Deletion Analyses

Total DNA was extracted from snap frozen QF samples by using standard phenol–chloroform extraction with ethanol precipitation method. MtDNA deletion load was determined by a semiquantitative long-template PCR amplification method (Ahola-Erkkilä et al., 2010) and also by triplex qPCR assay (Rygiel et al., 2015).

To determine the mtDNA deletion load, long-range mtDNA PCR was performed, with primers chosen from non-deleted mtDNA region between 16SrRNA and ND1 genes, enabling amplification of all the partly deleted molecules. For long range PCR, 10 ng of total DNA was amplified with the primers F-GAGGTGATGTTTTTGGTAAACAGGCGGGGT and R-GGTTCGTTTGTTCAACGAT TAAAGTCCTACGTG using Phusion high-fidelity DNA polymerase (Thermo Fisher # F530L) and GC buffer. The reaction conditions were as follows: initial denaturation of 30 s at 98°C; 22 cycles of 10 s at 98°C and 3 min at 72°C and final extension step for 10 min at 72°C. To determine the amount of total mtDNAs, we amplified a fragment from the non-deleted mtDNA region. The amount of the total mtDNA product was compared to the deleted mtDNA products. The primers F-ACCCCGCCTGTTTACCAAAAACATCACCTC and R-ACGTACCACTTTAATCGTTGAACAAACGAACC were used to produce a 549-kb product, using 10 ng of total DNA, Phusion high fidelity DNA polymerase and GC buffer. The PCR conditions were as follows: initial denaturation of 30 s at 98°C; 21 cycles of 10 s at 98°C and 3 min at 72°C; final extension step of 10 min at 72°C. All the PCR products were electrophoresed through 1% agarose gel. The gels were scanned by Typhoon 9400 fluorescence scanner (Amersham Biosciences) and products quantified by Image Quant (Amersham Biosciences) software.

The triplex assay was modified for mouse: we used specific murine primers, 3′-modified for stability. The probes for detection were 5′-modified with ROX (D-Loop probe), HEX (ND1 probe) or FAM (ND4 probe) for single-well detection. To determine primer efficiency the linear amplification range was determined by serial dilution and sample input DNA adjusted accordingly. A standard curve was included in every run. Primers pairs and probe sequences for mtDNA deletion analysis is available in Table S1.

mtDNA Copy Number Analysis

MtDNA copy number was analyzed from total DNA isolated from snap frozen QF samples, using the standard phenol chloroform and ethanol precipitation method. Twenty-five ng of total DNA template was used and the amplification product of mitochondrial *MTRNR1* (forward 5′-AGGAGCCTGTTCTATAATCGATAAA-3′ and reverse 5′-GATGGCGGTATATAGGCTGAA-3′) was normalized against the transcript amount of nuclear two-copy 18S gene (forward 5′-CGGACAGGATTGACAGATTG-3′ and reverse 5′-CAAATCGCTCCACCAACTAA-3′) by real-time quantitative PCR (Yatsuga and Suomalainen, 2012).

ATF4 Silencing Experiments

siRNA experiments were performed using SilencerSelect oligos (Sigma) against *ATF4* in two consecutive rounds using Polyplus jetPRIME transfection reagent. Cells were treated with actinonin (Sigma, A6671) for 16 hr before analysis.

Western Blotting

Total protein was extracted from QF muscle tissue samples, with 1% Triton-X in PBS and 1x Halt Phosphatase inhibitor cocktail (Thermo Fisher Scientific, #78420). Tissues were homogenized and whole-tissue lysates were prepared from a piece of QF in ice-cold 1x PBS containing Triton-X and 1x halt phosphatase inhibitor using a bead homogenizer (Precellys) with protease inhibitor (Complete Mini, Roche), followed by incubation on ice for 30 min. Protein concentration was measured using the Bradford method (Protein Assay, Bio-Rad). Ten micrograms of protein was loaded per well in SDS–PAGE and transferred to PVDF membranes and blocked with 5% milk or 3% BSA in 1x TBS-T for 1 hr and primary antibodies incubated overnight at 4°C at 1:1000 in 1% milk in TBS-T buffer. The list of antibodies is included in the Key Resources Table.

Gene Expression

Total cellular RNA was extracted from snap frozen muscle and heart tissues in TRIzol reagent (Invitrogen) and homogenized with Fast-Prep w-24 Lysing Matrix D (MP Biomedical) and Precellys w-24 (Bertin Technologies). Two micrograms of total RNA was used to generate cDNA using Maxima first-strand cDNA synthesis kit (#K1671; Thermo Scientific). Quantitative real-time PCR amplification of cDNA was performed with iQ SYBR Green qPCR kit (Biorad) on CFX96 Touch qPCR system (Bio-Rad). Relative expression of a transcript was determined by normalizing to the expression of housekeeping genes beta-actin and 18S rRNA. Primer sequences are provided in Table S1.

Metabolomics Data Analysis

Metabolite Extraction Protocol

For 100 metabolites analysis, approximately 20 mg of frozen muscle tissues were transferred to Precellys homogenizing tubes containing 1.4 mm ceramic (zirconium oxide) beads with 20 μL of labeled internal standard mix and 500 μL of 100% acetonitrile (ACN) and 1% formic acid (FA) as extraction solvent to all the tubes. Samples were homogenized using Precellys-24 homogenizer (Bertin Technologies, France) for three cycles, 20 s each, at 5,500 rpm; 30 s pause between each homogenization interval. After homogenization, the samples were centrifuged for 10 min, 5000 rpm, at 4°C in an Eppendorf 5404R centrifuge and the supernatant was collected. Same homogenization cycles were repeated after adding another 500μL of 90/10% CAN/H_2O+ 1% FA to the remaining pellet in homogenization tubes, both supernatants were pooled and filtered to Ostro™ plate by applying vacuum at delta pressure of

300 psi for 3-5 min. The clean extract was collected to a 96-well plate and was centrifuged for 15 min, 4000 rpm, 4°C and placed in auto-sampler of the liquid chromatography system for the injection (Nikkanen et al., 2016).

For folate intermediate analysis, around 40 mg of frozen tissue samples (QF) were weighed and homogenized as described above. A total of 20 μL of internal standard solution (400 ng\mL) was added and the samples were allowed to equilibrate on ice for 2 min. 450 μL of extraction buffer (HEPES buffer, pH 8.0) was added to the homogenization tubes and the samples were vortexed for 20 s. Tissue samples were homogenized using tissue homogenizer as above. After homogenization, 40 μL of charcoal-treated rat plasma was added, and samples were incubated at 37°C for 3 hr for folate deconjugation, followed by centrifugation at 14000 rpm for 15 min at 4°C. After centrifugation, 300 μL of supernatant was centrifuged again through 10 kDa cut off filter (Sartorius Stedim Biotech, Germany) at 14000 rpm for 30 min at 4°C and the filtrate was collected for injecting into chromatographic system for folate analysis.

Metabolomic Instrumentation and Analytical Conditions

Sample analysis was performed on an ACQUITY UPLC-MS/MS system (Waters Corporation, Milford, MA, USA). Chromatographic separation were done using the column, 2.1x100 mm Acquity 1.7μ BEH amide HILIC column and Atlantis dC18 reversed phase analytical column, 2.0 × 100mm, 3 μ particles (Waters Corporation, Milford, MA, USA), which were maintained at 45°C temperature for 100 metabolites and folate intermediate respectively. All 100 metabolites were separated in the total run time of 17 min at flow rate 600 μL/min and folate intermediates were separated in the total run time of 5 min at flow rate 300 μL/min. An injection volume of 5 μL of sample extract was used and two cycles of 300 μL of strong wash and 900 μL of weak wash and in addition 2 min of seal wash were carried out after each injection to avoid carry over effect. The auto-sampler was used to perform partial loop with needle overfill injections for the samples and standards and maintained at temperature of 5°C. The detection system, a Xevo TQ-S tandem triple quadrupole mass spectrometer (Waters, Milford, MA, USA), was operated in both positive and negative polarities with a polarity switching time of 20 msec. Electro spray ionization (ESI) was chosen as the ionization mode with a capillary voltage at 0.6 KV in both polarities. The source temperature and desolvation temperature of 120°C and 650°C, respectively, were maintained constantly throughout the experiment. Cone voltage and collision energy (CE) were optimized for each compound. High pure nitrogen and argon gas were used as desolvation gas (1000 L/hr) and collision gas (0.15 ml/min), respectively. Multiple Reaction Monitoring (MRM) acquisition mode was selected for quantification of metabolites with individual span time of 0.1 s given in their individual MRM channels. The dwell time was calculated automatically by the software based on the region of the retention time window, number of MRM functions and also depending on the number of data points required to form the peak. MassLynx 4.1 software was used for data acquisition, data handling and instrument control. Data processing was done using TargetLynx software and metabolites were quantified using area ratio (area of metabolite/area of IS) standards and external calibration curves.

The data has been autoscaled and missing values estimated by KNN using MetaboAnalyst 3.0 software (Xia et al., 2009). To analyze the differences among groups, univariate analyses, Student's t test and ANOVA were used. Separation among groups was tested by unsupervised multivariate analysis, principal component analysis (PCA).

dNTP Pool Measurement

For dNTP pool analysis, the Deletors and WT type mice, Vehicle and rapamycin injected, were sampled together and analyzed in parallel using sensitive polymerase-based assay as follows. QF muscle samples were weighed and homogenized in 10 volumes (v/w) of buffer containing 10 mM Tris/HCl, pH 7.5, 0.5% bovine serum albumin (BSA), 210 mM mannitol, 0.2 mM ethylene glycol tetra-acetic acid (EGTA) and 70 mM sucrose, using polytron homogenizer. Homogenates were then centrifuged at 1000 x g for 10 min at 4°C, and cold methanol (−20°C) was added to the supernatants to the final concentration of 60% (v/v). After incubation for 3 hr at −80°C, the samples were heated at 95°C for 3 min, cooled down on ice and then centrifuged at 16000 x g for 20 min at 4°C. The supernatants were transferred to new tubes and dried. The pellets were dissolved in cold water and stored at −80°C until further analysis. Appropriate amount of extracts or standards were added to a reaction mixture containing 40 mM Tris/HCl, pH 7.5, 10 mM $MgCl_2$, 5 mM dithiothreitol (DTT), 0.25 μM specific primed oligonucleotide, 0.75 μM ^{3}H-dTTP or ^{3}H-dATP, 0.30 unit Taq DNA polymerase in a total of 20 μL and incubated at 48°C for 60 min. 15 μL of the reaction mixture were spotted onto DE-81 filter paper, dried and washed three times with 5% Na_2HPO_4, once with water and once with 95% ethanol. The reaction products were quantified by liquid scintillation counting. Three to six measurements were performed for all samples individually (Nikkanen et al., 2016).

QUANTIFICATION AND STATISTICAL ANALYSIS

ImageJ software (NIH; Bethesda, MD, USA) was used for quantification of all histological samples. All statistical analysis was performed using Graphpad Prism 6.0 Software (Graphpad Software; La Jolla, CA, USA). The metabolomics data has been autoscaled and missing values estimated by KNN using MetaboAnalyst 3.0 software (Xia et al., 2009). Separation among groups was tested by unsupervised multivariate analysis, principal component analysis (PCA). Outlier analysis of metabolomics data was done using GraphPad Prism 6.0 ROUT method (Q = 1%) and false positive analysis in metabolomics with Benjamini-Hochberg method, critical value of 0.2.

Statistical significance was determined by unpaired Student's t test or ANOVA as mentioned in the figure legends.